The Astrophysical Journal, 872:88 (7pp), 2019 February 10 https://doi.org/10.3847/1538-4357/aafb30

Measuring the Circumgalactic and Intergalactic Baryon Contents with Fast Radio Bursts

Vikram Ravi
Cahill Center for Astronomy and Astrophysics, MC 249-17, California Institute of Technology, Pasadena, CA 91125, USA; vikram@caltech.edu
Received 2018 April 23; revised 2018 December 23; accepted 2018 December 27; published 2019 February 13

Abstract

Over 80% of the cosmic baryon density is likely to be distributed in the diffuse, $\gtrsim 10^4$ K circumgalactic and intergalactic medium (CGM and IGM, respectively). We demonstrate that the dispersion measures (DMs) of samples of localized fast radio bursts (FRBs) can be used to measure the distribution of baryons between the CGM and IGM. We propose to separate the CGM and IGM contributions to FRB DMs by including redshift and mass measurements of intervening galaxies. Using simulated samples of FRB sight lines through intervening galaxy halos and an illustrative model for the CGM, and including realistic observational uncertainties, we show that small samples (O(10^1)–O(10^2)) of localized FRBs are sensitive to the presence of CGM gas. The fractions of baryons in the CGM and IGM can be accurately estimated with a few tens of FRBs at $z < 1$, with uncertainties of $\sim$10% with $N = 10$ FRBs that decline as $N^{-1/2}$. The characteristic radial density profiles of CGM halos may also be possible to constrain with larger FRB samples. The required samples of localized FRBs are expected to be assembled in the coming few years by instruments such as the Australian Square Kilometre Array Pathfinder, the Deep Synoptic Array, MeerKAT, UTMOST-2D, and the Very Large Array.

Key words: cosmology: theory – galaxies: halos – intergalactic medium

1. Introduction

Up to 10% of the cosmic baryon fraction, Ω_b, is to be found in stars and the interstellar medium (ISM; Fukugita & Peebles 2004). The remainder is distributed between the circumgalactic medium (CGM; Tumlinson et al. 2017) and the filaments of the intergalactic medium (IGM; McQuinn 2016). However, in the redshift $z \sim 0$ universe, the bulk of the CGM ($\gtrsim$99% by mass) and the IGM ($\gtrsim$90%) is at temperatures $>10^4$ K and therefore largely ionized, making it difficult to observe. Quasar absorption-line studies in the rest-frame ultraviolet, probing H I and ionized-metal transitions corresponding to collisional and photoionization characteristic temperatures up to 10^6 K, paint a picture of largely mixed, multiphase, kinematically complex CGM/IGM gas. The hottest ($>10^6$ K) gas has been detected as extended X-ray thermal halos around nearby galaxies (e.g., Anderson et al. 2013) and through the thermal Sunyaev–Zel'dovich effect in IGM filaments (de Graaff et al. 2017; Tanimura et al. 2019). However, these studies rely on careful modeling of the density, temperature, and chemical profiles of the gas to derive total gas contents, making the overall fractions of Ω_b in the IGM ($f_{\rm IGM}$) and CGM ($\sim 1 - f_{\rm IGM}$) highly uncertain ($0.5 \lesssim f_{\rm IGM} \lesssim 0.9$; Shull et al. 2012; Werk et al. 2014). The dependence of CGM mass on halo mass is also poorly constrained by observations but may form a crucial discriminant between models for thermal and kinetic feedback in galaxies (Fielding et al. 2017; Suresh et al. 2017; Wang et al. 2017). Further, the characteristic radial density profile of the CGM is highly uncertain, although there are unsurprising indications that it is flatter in shape than the isothermal sphere case (Anderson et al. 2016; Prochaska et al. 2017).

Understanding the distribution of baryons within and between the CGM and IGM is a fundamental astronomical problem, with critical implications for the growth mechanisms of galaxies from extragalactic gas. Here we consider whether detailed observations of fast radio burst (FRB) sight lines can be used to measure (a) the CGM/IGM baryon fractions (parameterized by $f_{\rm IGM}$) and (b) the radial density profiles of the CGM ($\rho_{\rm CGM}(r)$, where r is the galactocentric radius). FRBs are extragalactic gigahertz-frequency events of micro- to millisecond durations, characterized by delays due to dispersion in intervening free-electron columns well in excess of Galactic expectations for their sight lines. FRBs are found with estimated extragalactic free-electron column densities (parameterized by the dispersion measure, or DM) of between 75 and 2600 pc cm^{-3}. In this paper, where applicable the extragalactic DM is defined as the difference between the measured FRB DM and the expected DM contributed by the Milky Way disk (Lorimer et al. 2007; Thornton et al. 2013), according to the NE2001 model (Cordes & Lazio 2002). If the extragalactic DMs are modeled as primarily arising in the IGM (Ioka 2003; Inoue 2004), FRB redshifts of between 0.01 and 2 are suggested (Dolag et al. 2015; Shull & Danforth 2018). However, non-negligible contributions to extragalactic DMs from FRB host galaxies are also possible and indeed favored by some FRB models (e.g., Kulkarni et al. 2015; Connor et al. 2016; Yang et al. 2017; Walker et al. 2018). In the case of the repeating FRB 121102 (with an extragalactic DM of $\sim$340 pc cm^{-3}) localized to a star-forming region of a $z = 0.193$ dwarf galaxy (Chatterjee et al. 2017; Tendulkar et al. 2017), the host DM contribution was limited to be $\lesssim$250 pc cm^{-3}, assuming that the associated Hα-emitting nebula traced the entire host DM (Kokubo et al. 2017). Other FRBs are unlikely to originate in magneto-ionic environments as extreme as that of FRB 121102 (Bassa et al. 2017; Michilli et al. 2018). For example, the sparsely populated localization region of the ultrabright FRB 150807 (extragalactic DM of $\sim$200 pc cm^{-3}) suggested a distance in excess of 500 Mpc, and its low Faraday rotation measure in comparison with its scattering properties suggested a host ISM unlike even that of the Milky Way (Ravi et al. 2016).

We focus on the prospects for FRBs that are localized to individual host galaxies, such that host and intervening galaxy redshift measurements are possible. Samples of a few hundred FRBs localized with sufficient (few arcseconds; Eftekhari & Berger 2017) accuracy upon the first instances of their detection

are expected in the coming few years from the Australian Square Kilometre Array Pathfinder (ASKAP; Bannister et al. 2017), the Deep Synoptic Array (DSA; V. Ravi et al. 2019, in preparation), MeerKAT (Sanidas et al. 2018), UTMOST-2D (Bailes et al. 2017), and the *realfast* system at the Jansky Very Large Array (VLA; Law et al. 2018). Although these surveys are well motivated by the problem of FRB progenitors, we argue that they may further result in impactful insights into the CGM/IGM. Our work builds on previous studies of similar intent by McQuinn (2014), Deng & Zhang (2014), and Zheng et al. (2014). However, our approach is distinct from these works in that we consider what may be achieved with redshift measurements of FRB host galaxies together with redshift and mass estimates for a sample of intervening galaxies. Our simulations of samples of FRBs and intervening galaxy halos are described in Section 2. The aim of the simulations is to ascertain whether a sample of $N_{\rm FRB}$ FRBs, each with host and intervening galaxy measurements, can be used to estimate $f_{\rm IGM}$ and $\rho_{\rm CGM}(r)$. We hypothesize that this can be done by comparing measurements of the summed CGM and IGM components of FRB DMs, $\rm DM_{EG}$, with predictions given the redshifts and masses of intervening galaxy halos and the FRB redshifts. We demonstrate the potential of this technique with simulations of observed FRB samples in Section 3, and we summarize and discuss our results in Section 4. We adopt the latest Planck cosmological parameters (Planck Collaboration et al. 2016), with a Hubble constant of $H_0 = 67.7\,{\rm km\,s^{-1}\,Mpc^{-1}}$, $\Omega_b = 0.0486$, matter density parameter $\Omega_M = 0.3089$, dark energy density parameter $\Omega_\Lambda = 0.6911$, and density fluctuation parameter $\sigma_8 = 0.8159$.

2. The Simulation

This section describes how we generate a sample of FRB sight lines through the CGM and IGM. First, we adopt a uniform distribution for observed FRB redshifts. The lack of FRB redshift measurements besides FRB 121102, combined with the uncertain relation between DM and redshift and unknown characteristic host DM contributions, means that it is difficult to observationally motivate a specific FRB redshift distribution. Furthermore, current FRB observations suggest a relation between FRB fluence and DM, which may be interpreted as a relation between fluence and redshift (Shannon et al. 2018). This would imply that the observed FRB redshift distribution depends on the specific fluence threshold. From a theoretical standpoint, the FRB redshift distribution observed at a specific frequency above a fixed detection threshold is determined by the FRB luminosity function, intrinsic spectrum, and evolution (or lack thereof) in the volumetric FRB rate with redshift (e.g., Macquart & Ekers 2018; Ravi & Loeb 2018). The latter quantities are themselves difficult to predict, given the wide range of extant FRB progenitor models (Platts et al. 2018), and are difficult to deduce from the current FRB sample (e.g., Caleb et al. 2016). Our assumption of FRB samples that are uniformly distributed in redshift mitigates these uncertainties.

The FRB redshift distribution only affects our results inasmuch as the range of simulated FRB sight lines used to constrain $f_{\rm IGM}$ and $\rho_{\rm CGM}(r)$ is concerned. In the coming sections, we largely consider FRBs observed at redshifts $z < 1$. With this restriction, we have determined that there is negligible difference in our results between choosing a uniform FRB redshift distribution and choosing one that matches the star formation rate (which approximately scales as $(1+z)^3$; Hopkins & Beacom 2006).

The next ingredient of the simulation is to specify the statistics of intervening galaxy halos along each FRB sight line. That is, for an FRB at a redshift $z_{\rm FRB}$, the distribution of intervening galaxy halos in their masses, M_h, and redshifts, z, needs to be defined. To define the angular size of a halo on the sky, we approximate the extent of each halo by its (approximate) virial radius, r_{200} (Cole & Lacey 1996). Following the usual convention, this is the radius at which the matter density is 200 times the cosmological critical density. We adopt a Navarro–Frenk–White (NFW; Navarro et al. 1996) halo density profile and Duffy et al. (2008) concentration parameters, to calculate the virial radii, $r_{200}(M_h, z)$, for halos of different masses at different redshifts. This calculation is implemented in the publicly available `NFW` software package.[1] The halo-mass function, $dn(M_h, z)/dM_h$, is in turn specified according to Sheth et al. (2001), as implemented by Murray et al. (2013) in the `hmf` software package. Then, the number of halos intercepted per unit halo mass, per unit redshift, by an arbitrary sight line is given by

$$\frac{d^2N}{dM_h\,dz} = 4\pi r_{200}^2(M_h, z)\frac{dn(M_h, z)}{dM_h}\frac{c(1+z)^2}{H(z)}, \qquad (1)$$

where c is the vacuum speed of light and $H(z)$ is the Hubble parameter. This equation mirrors Equation (31) of Hogg (1999), which quantifies the probability of intersecting objects along cosmological sight lines.

For each FRB sight line to a redshift $z_{\rm FRB}$, we use the distribution function in Equation (1) to randomly draw a sample of intervening halos. This is done using the rejection sampling technique (Press et al. 2007). Throughout this work, we only consider halo masses in the range of 10^{11}–$10^{15}\,M_\odot$. The CGM contents of lower-mass halos, corresponding to stellar masses $\lesssim 10^9\,M_\odot$ (Behroozi et al. 2010), are unlikely to be maintained in thermal equilibrium by virial shocks and are therefore strongly influenced by galactic feedback mechanisms (Fielding et al. 2017). Many simulations (e.g., Schaller et al. 2015; Wang et al. 2017) find that feedback in low-mass halos results in smaller CGM mass fractions than in higher-mass halos (although see Suresh et al. 2017), in tentative agreement with observations (Tumlinson et al. 2017). Further, the baryonic components of halos with masses $<10^{10}\,M_\odot$ are below the IGM Jeans mass and are unlikely to have collapsed. These arguments, together with the statistics of halo intercepts specified by Equation (1), suggest that the contributions of the CGM in $M_h < 10^{11}\,M_\odot$ halos to FRB DMs may not be significant. Further, halos with masses $\gtrsim 10^{15}\,M_\odot$ host galaxy clusters rather than individual large galaxies and have intracluster medium properties that are beyond the scope of this work to constrain. The probability of an arbitrary FRB sight line to $z = 1$ intersecting a $\gtrsim 10^{15}\,M_\odot$ halo within its virial radius is 7×10^{-4}. We therefore do not consider such massive halos in this work.

Having obtained a sample of FRB sight lines each with a sample of intercepted halos, we next need to specify the DM contributions from the CGM in each halo. In this work, we consider two illustrative boundary case models for $\rho_{\rm CGM}(r)$ to calculate these DM contributions. In the first model (Model A), we assume a constant-density CGM within the virial radius (i.e., at $r < r_{200}$). In the second model (Model B), we assume

[1] https://github.com/joergdietrich/NFW

an isothermal sphere truncated at the virial radius, such that $\rho_{\rm CGM}(r) \propto r^{-2}$ for $r < r_{200}$. These two models bound the tentatively measured dependency of $\rho_{\rm CGM}$ on r (Anderson et al. 2016; Prochaska et al. 2017) and also bound results from simulations (Fielding et al. 2017) that suggest $\rho_{\rm CGM}(r) \propto r^{-1.5}$. At each redshift, we derive a normalization constant for the halo radial density profiles by requiring that the total CGM mass of each halo be given by $(1 - f_{\rm IGM})M_h\Omega_b/\Omega_{M>11}$, where $\Omega_{M>11}$ is the fraction of the critical density in $M_h > 10^{11}\,M_\odot$ halos. We neglect the fraction of Ω_b in stars and the ISM; this is justified because our analysis is agnostic to the actual fractions of Ω_b in the CGM and IGM. The electron densities at each redshift are calculated following Equation (1) of Shull & Danforth (2018), together with the assumption of no significant difference in the ionization fractions of the CGM and IGM. To specify the actual DM contributions from each halo along each FRB sight line, we randomly draw the impact parameters of the FRB sight lines with respect to the intervening halos from a probability density function proportional to r. This is the expectation for a uniform distribution of 2D projected separations between FRB sight lines and halo centers. We also correct the rest-frame DM contributions of each halo by a factor of $(1 + z)^{-1}$ to account for the redshifting of FRB emission.

For the purposes of our simulations, we define a $\rm DM_{EG}$ that is the sum of the CGM and IGM contributions to FRB DMs. To specify the IGM contributions to $\rm DM_{EG}$, we adopt the formalism of Shull & Danforth (2018) for the DM contribution from a constant-density IGM (their Equations (4) and (5), but corrected to include a factor of $(1 + z)^{-1}$ in the integrand of Equation (5)). Shull & Danforth (2018) suggest an intrinsic scatter of $\sigma_{\rm IGM} \approx 10\,{\rm pc\,cm^{-3}}$, which we adopt, to account for cosmic-web voids and filaments.

In Figure 1, we show simulations of the CGM and IGM contributions to $\rm DM_{EG}$ for 1000 FRB sight lines at various redshifts in the range $z = 0$–2, assuming $f_{\rm IGM} = 0.5$. Our assumption of $f_{\rm IGM} = 0.5$ in panels (b) and (c) of the figure implies typical CGM DM contributions of a few hundred $\rm pc\,cm^{-3}$ for FRBs beyond $z = 1$ (panel (b)), while the fractional contribution of the CGM to $\rm DM_{EG}$ is largest for lower redshifts. For the purposes of illustration, no scatter has been included in the IGM DMs in panel (b). Panel (c) indicates that Model A CGM radial density profiles (constant density) result in typically larger CGM DMs than Model B profiles (isothermal sphere), which is expected given the greater concentration of baryons within halos in Model B. For an approximate comparison with observations, we show (panel (a)) a histogram of the extragalactic DMs of the observed FRB sample (as tabulated in the FRB Catalog; Petroff et al. 2016) converted to redshifts assuming that the extragalactic DMs arise entirely in the IGM and adopting the redshift–DM relation of Shull & Danforth (2018) as above, but assuming $f_{\rm IGM} = 1$. The observed FRB sample likely probes redshifts $z_{\rm FRB} < 1$, in the regime where the fractional contributions of the CGM to $\rm DM_{EG}$ are large but highly uncertain.

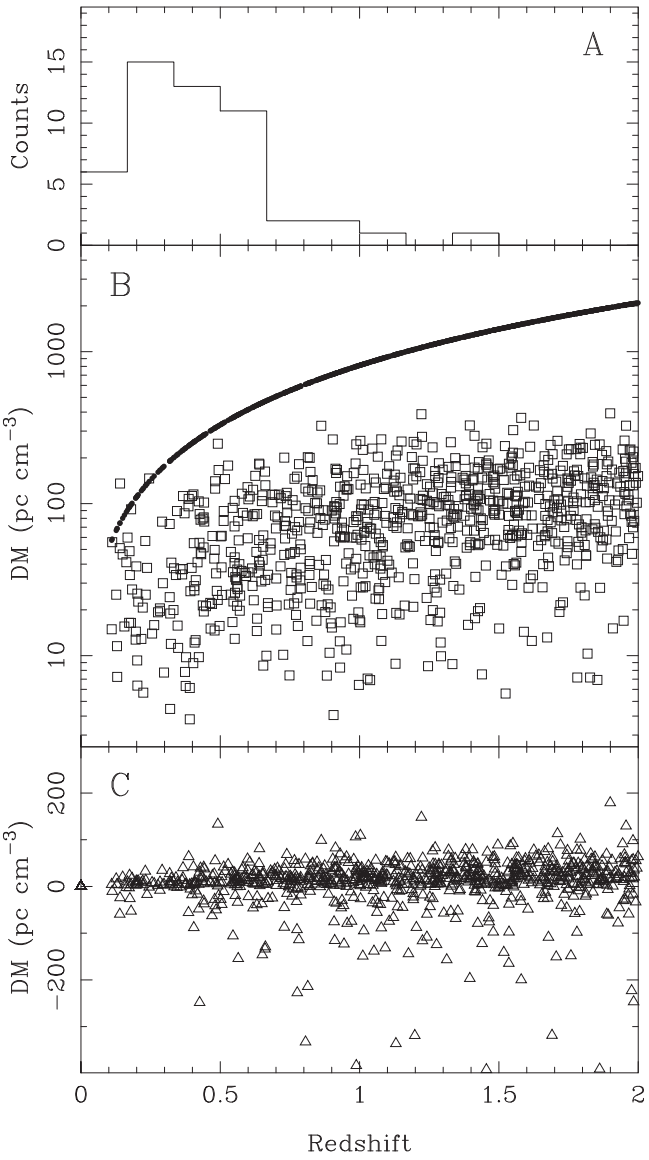

Figure 1. (a) Histogram of the approximate redshifts (see text for details) of the 51 currently cataloged FRBs. (b) Contributions to FRB DMs from the IGM (open circles; no scatter included) and CGM (open squares) for 1000 simulated FRB sight lines. We adopted the Model A (constant-density) CGM radial density profile and assumed $f_{\rm IGM} = 0.5$. Note that the results for other values of $f_{\rm IGM}$ can be derived through a straightforward linear scaling by $f_{\rm IGM}/0.5$. (c) Difference between the DM contributions from the CGM for Model A and B (isothermal sphere) CGM density profiles. Model A profiles result in typically larger CGM DM contributions.

3. Results

We use the simulations described above to ascertain whether $f_{\rm IGM}$ and $\rho_{\rm CGM}(r)$ can be estimated using samples of localized FRBs. The method we propose is to compare measurements of the summed CGM+IGM FRB DMs, $\widehat{\rm DM}_{\rm EG}$, with predictions for $\rm DM_{EG}$. The predictions, which are based on redshift and mass measurements of intervening galaxies and measurements of FRB redshifts, depend on an assumed $f_{\rm IGM}$ to partition free electrons between the CGM and IGM and on an assumed $\rho_{\rm CGM}(r)$ to calculate the DM contributions from each intervening galaxy halo. Thus, measurements of $\widehat{\rm DM}_{\rm EG}$ will only be consistent with predictions of $\rm DM_{EG}$ for a unique combination of $f_{\rm IGM}$ and $\rho_{\rm CGM}(r)$.

We first consider how samples of FRBs with identified intervening galaxies are assembled in practice. Potential sources of error in both the estimates of and predictions for the CGM/IGM DMs are assessed. We then demonstrate the

effects of these errors on estimates of $f_{\rm IGM}$ and $\rho_{\rm CGM}(r)$ using realistic samples of localized FRBs.

3.1. Observational Considerations

Constructing the estimate $\widehat{\rm DM}_{\rm EG}$ for an observed FRB relies on subtracting all other contributions from the measured DM. Each subtraction has a corresponding uncertainty. First, FRB DM contributions from the Milky Way disk are traditionally estimated by integrating the NE2001 model for the warm ionized medium density structure (Cordes & Lazio 2002) to its outer edge, resulting in values of $\sim 30/\sin|b|$ pc cm^{-3} at high Galactic latitudes b. Negligible uncertainty is expected in these estimates for $|b| \gtrsim 20^\circ$ (Gaensler et al. 2008; Dolag et al. 2015). Next, the Milky Way hot halo (i.e., its CGM) is expected to produce $\sim$40 pc cm^{-3} of DM for every FRB, with an uncertainty of $\sigma_{\rm MW} \approx 15$ pc cm^{-3} (Dolag et al. 2015). DM contributions from FRB host galaxies are highly uncertain and dependent on specific progenitor models (Xu & Han 2015; Yang et al. 2017; Walker et al. 2018). Here we assume that as larger samples of localized, thoroughly characterized FRBs are constructed, further insight into FRB progenitors will be gleaned from, for example, their host galaxies, positions with respect to their hosts, characteristic luminosities, spectra, polarizations, scattering and Faraday rotation properties, repeatability, and potential multi-wavelength counterparts. Further, given that exceedingly large host DM contributions are likely excluded in some known cases (Ravi et al. 2016), we assume that host galaxy DMs can be subtracted with a conservative uncertainty of $\sigma_{\rm host} \approx 50$ pc cm^{-3} (e.g., Figure 3 of Walker et al. 2018). Adding $\sigma_{\rm MW}$, $\sigma_{\rm host}$, and $\sigma_{\rm IGM} \approx 10$ pc cm^{-3} (see above) in quadrature results in an uncertainty of $\sigma_{\rm EG} \approx 53$ pc cm^{-3}.

Predicting ${\rm DM}_{\rm EG}$ for an FRB sight line relies on observationally identifying intervening galaxy halos and measuring their redshifts and masses. We consider a scheme whereby candidate intervening galaxies are identified through optical/IR imaging, perhaps including color information to estimate photometric redshifts, and spectra are obtained using multi-object spectrographs to confirm redshifts. Intervening galaxies widely separated from FRB sight lines are unlikely: for example, the sample of 1000 FRB sight lines presented in Figure 1 contains only eight intervening galaxies with projected offsets $>10'$, with a maximum offset of $16\farcm1$, out of 3114 intervening galaxies. To assess the completeness of imaging observations of specific depths to intervening galaxies, we assign optical/IR spectral energy distributions (SEDs) to simulated intervening dark matter halos using the publicly available output catalogs of a recent semianalytic galaxy formation model (Henriques et al. 2015). We obtained rest-frame dust-corrected SEDs between the *GALEX*–far-UV and K bands for halos in the mass range of 10^{11}–$10^{15}\,M_\odot$ for each redshift snapshot and binned them in 0.04 dex M_h bins. For each simulated intervening halo, we then randomly drew an SED from the nearest mass and redshift bin, K-correcting the observed SED and accounting for the halo luminosity distance. We consider two means of selecting candidate intervening systems for spectroscopic follow-up: detection in four of the five filters of the Pan-STARRS1 3π survey stack (PS1; Chambers et al. 2016), and detection in an r-band image with $m_r < 24$ (AB).

In Figure 2, we show the impact of these observational selections on the typical completeness of intervening galaxy samples for FRBs at various redshifts. We present the mean fractions of the total CGM DMs for FRBs in 10 redshift bins in the range $z = 0$–3 recovered by the two observational selections. For example, for a $z < 1$ FRB, >50% of the CGM DM is expected on average to be contributed by galaxies detected in four PS1 filters. For a $z < 0.5$ FRB, r-band imaging observations with a limiting magnitude of $m_r = 24$ will detect galaxies contributing on average >90% of the CGM DM.

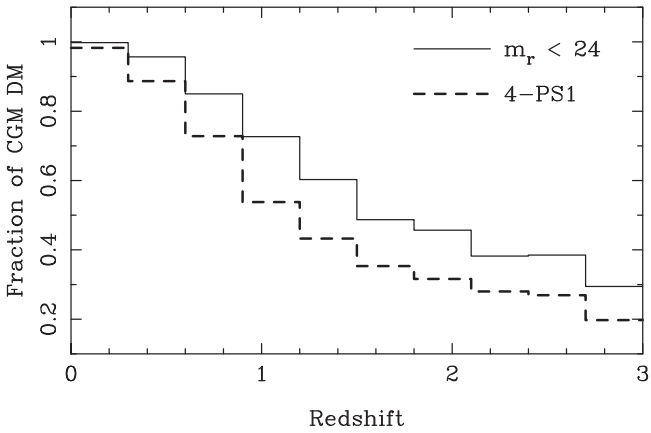

Figure 2. Demonstration of the impacts of observational limitations in identifying intervening galaxies on estimates of CGM DM contributions to ${\rm DM}_{\rm EG}$. The curves show the mean fractions of FRB CGM DMs contributed by observed intervening galaxies in 10 bins of redshift. Two observational schemes are considered: the case where galaxies are identified with apparent r-band magnitudes $m_r < 24$ (solid curve), and the case where detections in four of the five Pan-STARRS1 3π-survey stack filters are required (Chambers et al. 2016; dashed curve). Although Model A (constant-density) CGM density profiles were assumed, adopting Model B profiles does not significantly alter the results.

In estimating dark matter halo masses, the tight relation between halo and stellar masses (intrinsic scatter ≈ 0.16 dex; Behroozi et al. 2010) implies that stellar-mass estimation errors can predominantly contribute to halo-mass errors. Based on the assessment of the stellar-mass estimation error budget by Mobasher et al. (2015), we consider stellar-mass estimation errors of 0.25 dex. In particular, we assume that deep follow-up imaging renders photometric errors negligible, and that the existence of spectroscopic data on each galaxy enables the accurate modeling of nebular emission lines. Thus, our total scatter in halo-mass estimates is 0.3 dex.

3.2. Estimating $f_{\rm IGM}$ and $\rho_{\rm CGM}(r)$

We consider a maximum likelihood estimate of $f_{\rm IGM}$ and $\rho_{\rm CGM}(r)$ given a sample of FRB sight lines, where each FRB i is accompanied by measurements of $\widehat{\rm DM}^i_{\rm EG}$ and predictions of ${\rm DM}^i_{\rm EG}(f_{\rm IGM}, \alpha)$. For the purposes of estimation, we adopt the parameterization $\rho_{\rm CGM}(r) \propto r^\alpha$. Assuming normally distributed errors with variance $\sigma^2_{\rm DM}$, the likelihood function is specified by

$$\mathcal{L}(f_{\rm IGM}, \alpha) \propto \prod_i \exp[-(\widehat{\rm DM}^i_{\rm EG} - {\rm DM}^i_{\rm EG})^2/(2\sigma^2_{\rm DM})]. \quad (2)$$

We demonstrate the estimation of $f_{\rm IGM}$ and α by numerically evaluating this likelihood function in two cases:

Case 1: True values of $f_{\rm IGM} = 0.8$ and $\alpha = 0$ (Model A CGM density profiles). Intervening galaxies are first identified in an r-band image with a limiting magnitude of $m_r = 24$.

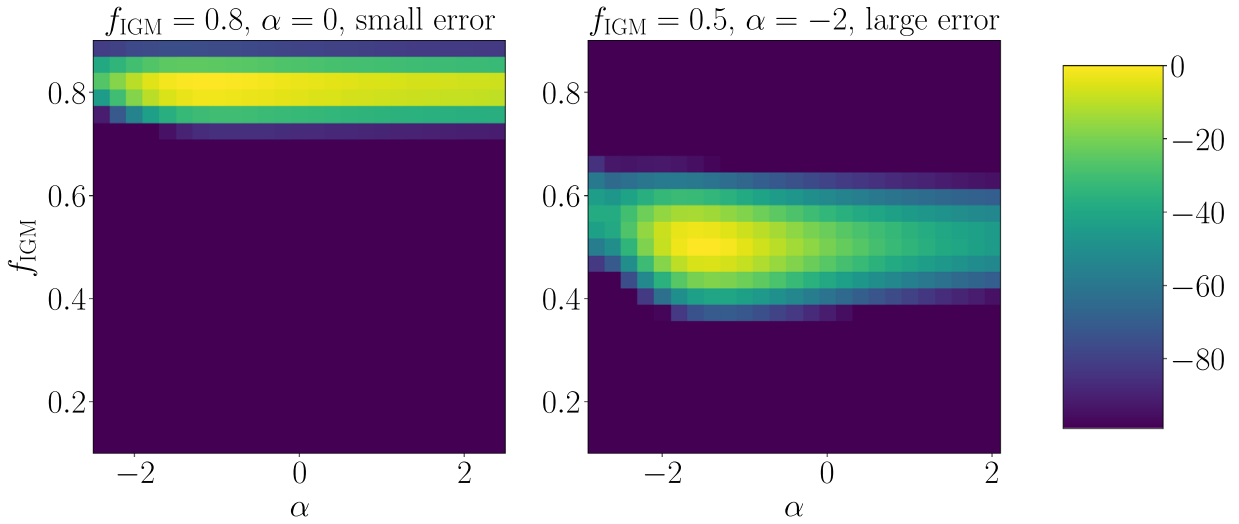

Figure 3. Each panel depicts the relative (natural) log-likelihood in the $f_{\rm IGM}$–α plane for individual simulated samples of 100 FRBs. Left: Case 1 sample (see text for details). Right: Case 2 sample. The true values of $f_{\rm IGM}$ and α are indicated above each panel.

Case 2: True values of $f_{\rm IGM} = 0.5$ and $\alpha = -2$ (Model B CGM density profiles). Intervening galaxies are first identified using detections in four PS1 filters. We also assume that a further 0.3 dex of uncertainty is combined with the scatter in the CGM density predictions for each intervening galaxy owing to potential unmodeled galaxy-to-galaxy variations in CGM mass.

We evaluate the likelihood for various trial pairs of $f_{\rm IGM}$ and α in each case using simulated FRB samples. In each sample, "measurements" $\widehat{\rm DM}^i_{\rm EG}$ are generated by first calculating the true values of the CGM/IGM DMs for each sight line for the assumed $f_{\rm IGM}$ and α and then adding normally distributed error values with zero mean and standard deviation $\sigma_{\rm EG} = 53\,{\rm pc\,cm^{-3}}$. For each pair of trial values of $f_{\rm IGM}$ and α, predicted CGM contributions to ${\rm DM_{EG}}$ are generated by drawing a random sample of observed intervening galaxies to calculate the CGM DM. We correct each prediction based on the estimated completeness factor for the FRB redshift (as depicted in Figure 2) and include lognormally distributed errors with standard deviations of 0.3 dex (Case 1 above) and 0.42 dex (Case 2). Predicted IGM contributions to ${\rm DM_{EG}}$ are calculated as described in Section 2 with no errors added (these errors are absorbed in the $\widehat{\rm DM}^i_{\rm EG}$ simulations). We estimate the variances $\sigma^2_{\rm DM}$ for a given sample by calculating the variance of $\widehat{\rm DM}^i_{\rm EG} - {\rm DM}^i_{\rm EG}$ values, where the predictions ${\rm DM}^i_{\rm EG}$ were made with the true values of $f_{\rm IGM}$ and α. In both cases, we limit our simulated samples to $z < 1$ to ensure reasonable completeness of the intervening galaxy observations to the CGM DM contributions; most currently observed FRBs are likely to originate from $z < 1$ (e.g., Dolag et al. 2015; Shull & Danforth 2018).

In Figure 3, we show the relative log-likelihoods in the $f_{\rm IGM}$–α plane for realizations of 100 FRB samples in Cases 1 and 2. High-significance measurements of $f_{\rm IGM}$ are possible in both cases regardless of the value of α, whereas only a weak constraint on α, equivalent to a lower limit, is possible in Case 1. Further simulations that we conducted showed that no useful constraints are possible on α in Case 2. The difference in the α-constraints between the cases is due to a combination of the increased uncertainty and lower value of α in Case 2.

The greater sensitivity of the technique to $f_{\rm IGM}$ as compared to α is because the variation in the predicted CGM DM with halo impact parameter for different values of α is weaker than the variation in ${\rm DM_{EG}}$ with $f_{\rm IGM}$, within the allowed ranges. This is demonstrated in Figure 4. Here, for a sample of 100 FRBs in Case 1, the measured values of ${\rm DM_{EG}}$ (i.e., $\widehat{\rm DM}_{\rm EG}$) are compared with erroneous predictions of ${\rm DM_{EG}}$: a large variation in α (correct $f_{\rm IGM} = 0.8$ but wrong $\alpha = -2$; open squares) and a small variation in $f_{\rm IGM}$ (wrong $f_{\rm IGM} = 0.6$ and correct $\alpha = 0$; asterisks). The ordinate in Figure 4 shows the differences between the erroneous predictions of ${\rm DM_{EG}}$ and the $\widehat{\rm DM}_{\rm EG}$ values, which feed directly into the calculation of the likelihood in Equation (2). Varying the input value of α from 0 to -2 only has a small effect on the errors in predicting ${\rm DM_{EG}}$, with the ${\rm DM_{EG}}$ values of FRBs at high redshifts being marginally underpredicted owing to the increased concentration of halo baryons with $\alpha = -2$. On the other hand, varying the input value of $f_{\rm IGM}$ from 0.8 to 0.6 causes a significant underprediction of the ${\rm DM_{EG}}$ values of higher-redshift FRBs. This is because the fractional contribution to ${\rm DM_{EG}}$ from the IGM increases with redshift, and lower values of $f_{\rm IGM}$ lock more baryons into the stochastically sampled CGM.

To better quantify the utility of localized FRB samples of different sizes, we refer the reader to Figure 5. Here we plot the uncertainties (95% confidence intervals, or ± 2 standard deviations) in estimating $f_{\rm IGM}$ in Cases 1 and 2 for FRB samples of different sizes, marginalized over α. By running simulations in the range $10 < N_{\rm FRB} < 1000$, we verified that the uncertainty in $f_{\rm IGM}$ is proportional to $N_{\rm FRB}^{-1/2}$. This is not a trivial result, because it depends on whether or not the CGM DM contributions are typically dominated by the largest, rarest intervening halos. This appears not to be the case, as is further indicated by the spread of CGM DM contributions in Figure 1 (b). We find that the uncertainty in $f_{\rm IGM}$ is given by $0.061 N_{\rm FRB}^{-1/2}$ in Case 1 and $0.099 N_{\rm FRB}^{-1/2}$ in Case 2. These results are highly promising: even in Case 2, an estimate of $f_{\rm IGM}$ with an uncertainty of 0.05 is likely possible with $N_{\rm FRB} = 100$.

4. Summary and Discussion

We present realizations of cosmological FRB sight lines through intervening galaxy halos, with the aim of determining

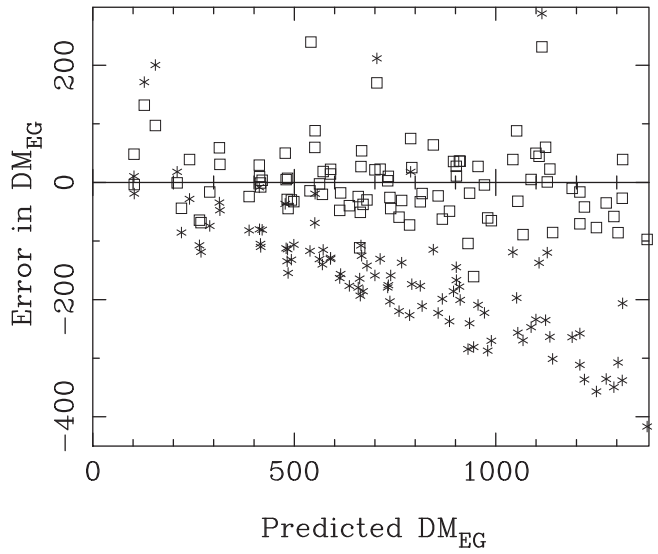

Figure 4. Differences between predicted and "measured" values of DM_{EG} for a sample of 100 FRBs in Case 1, where errors have been introduced into the predictions. The squares show a scenario where f_{IGM} is held fixed at 0.8 but α has been varied from 0 to −2. The asterisks show a scenario where f_{IGM} has instead been varied from 0.8 to 0.6, with α held fixed at the correct value of 0.

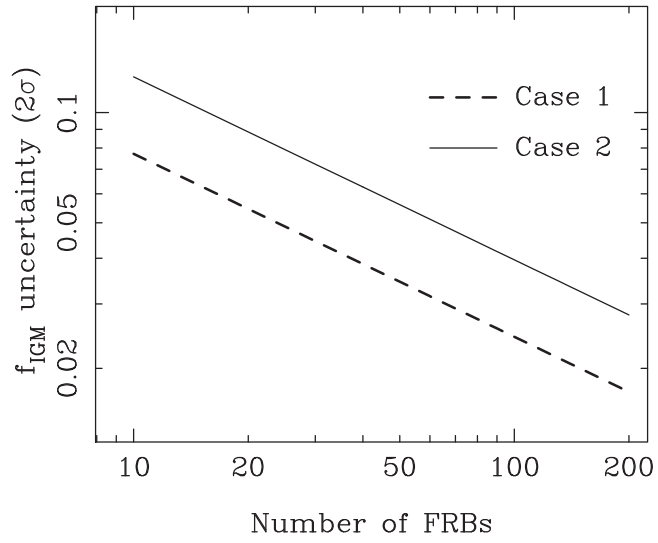

Figure 5. Uncertainties in estimating f_{IGM} (95% confidence intervals) in Cases 1 and 2 (see text for details) for FRB samples of different sizes.

whether samples of localized FRBs are sensitive to the presence of circumgalactic gas. By parameterizing the fractions of Ω_b in the IGM and CGM as f_{IGM} and $1 - f_{IGM}$, respectively, and assuming power-law CGM radial density profiles of the form r^{α}, we find that f_{IGM} can be accurately estimated, and weak constraints potentially placed on α, with 100 FRBs at $z < 1$ (Figure 3). Almost independently of the value of α, useful measurements of f_{IGM} can be obtained using samples of $N_{FRB} > 10$ localized events (Figure 5). Our work differs from previous studies (e.g., McQuinn 2014) in that we assume that each FRB is accompanied by a redshift measurement, and that follow-up observations are conducted to measure the redshifts and masses of intervening galaxies (Section 3.1). The initial identification of intervening galaxies in a survey such as the Pan-STARRS 3π stack is sufficient to recover on average >50% of our simulated CGM contributions to FRBs at $z < 1$ (Figure 2).

The ASKAP, VLA/*realfast*, and DSA surveys are together expected to yield up to 100 FRBs localized to individual galaxies in the coming 3–5 yr, with a significant fraction at $z < 1$. For example, the DSA will have a system-equivalent flux density for FRB searching within a factor of two of the Parkes telescope, but with a primary beam that is a factor of 12 larger in area (V. Ravi et al. 2019, in preparation). The DSA is a dedicated FRB search/localization instrument under construction at the Owens Valley Radio Observatory, with full operations planned to commence by the end of 2020. We are likely to have a sufficiently large localized FRB sample in hand over the next few years to accurately estimate f_{IGM}.

However, substantial optical follow-up of each FRB sight line will be required to realize our goal of characterizing the bulk baryon contents of the CGM and IGM. For example, if intervening galaxies were to be selected in deep r-band images above a limiting magnitude of $m_r = 24$, ∼25 galaxies arcmin^{-2} (Smail et al. 1995) would have to be sifted through in a few × few arcminute region to identify <10 intervening galaxies. Initial selections based on photometric redshifts may enable the intervening galaxies to be identified using individual ∼2 hr multislit spectroscopic observations with 8m class telescopes; these will ultimately be available over large areas of the sky from the Large Synoptic Survey Telescope and the Dark Energy Spectroscopic Instrument data sets.

In practice, analyses such as that we propose may be affected by a selection of systematic uncertainties beyond those included in our simulations. Measurements of the combined CGM and IGM components of FRB DMs ($\widehat{DM}_{EG}$) rely on accurate subtraction of other DM components. First, the scatter in host galaxy DMs may need to be mitigated by the careful selection of FRB samples. For example, it may be necessary to exclude FRBs with similar host environments to the repeating FRB 121102, for which DMs up to ∼250 pc cm^{-3} could be contributed by the host (Kokubo et al. 2017; Tendulkar et al. 2017), unless a way to more accurately measure host DMs were found. Even without the $\ll 1''$ localization accuracy required to associate FRB 121102 with a star-forming region, similar FRBs could be identified by, e.g., the host galaxy properties or their Faraday rotation measures. Second, more scatter than we have assumed may be present in "IGM" DMs if, for example, $M_h < 10^{11}\,M_{\odot}$ halos retain significant baryon fractions. On the other hand, the statistics of FRB DMs may instead be useful in identifying any unknown sources of DM associated with FRB sight lines, such as dense progenitor environments (e.g., Walker et al. 2018). Finally, a more refined analysis would include the effects of galaxy clustering in specifying the occurrence of intervening galaxy halos along FRB sight lines.

Samples of localized FRBs may provide the best means to determine the distribution of baryons within and between the CGM and IGM. Motivated by the promising results presented here, we will extend this work in a forthcoming paper by analyzing FRB sight lines in cosmological galaxy formation simulations. Several improvements to our model for the CGM and IGM DMs are desirable, such as a self-consistent treatment of baryon fractions in stars/dust and multitemperature gas; the consideration of more sophisticated CGM density structures, extents, and masses that may all vary with galaxy mass and type; and a robust prescription for baryon density fluctuations outside galaxies and galaxy clustering. The possibility of FRB observations being affected by and gaining insights into these

complexities further motivates the assembly of large samples of localized events.

We thank G. Hallinan, P. Hopkins, C. Hummels, and H. Vedantham for useful discussions and J. Hessels for comments on the manuscript. We made use of the `astropy` (http://www.astropy.org/), `hmf` (Murray et al. 2013), and `NFW` (https://github.com/joergdietrich/NFW) Python packages in this work. The Millennium Simulation database used in this paper and the web application providing online access to them were constructed as part of the activities of the German Astrophysical Virtual Observatory.

ORCID iDs

Vikram Ravi https://orcid.org/0000-0002-7252-5485

References

Anderson, M. E., Bregman, J. N., & Dai, X. 2013, ApJ, 762, 106
Anderson, M. E., Churazov, E., & Bregman, J. N. 2016, MNRAS, 455, 227
Bailes, M., Jameson, A., Flynn, C., et al. 2017, PASA, 34, e045
Bannister, K. W., Shannon, R. M., Macquart, J.-P., et al. 2017, ApJL, 841, L12
Bassa, C. G., Tendulkar, S. P., Adams, E. A. K., et al. 2017, ApJL, 843, L8
Behroozi, P. S., Conroy, C., & Wechsler, R. H. 2010, ApJ, 717, 379
Caleb, M., Flynn, C., Bailes, M., et al. 2016, MNRAS, 458, 708
Chambers, K. C., Magnier, E. A., Metcalfe, N., et al. 2016, arXiv:1612.05560
Chatterjee, S., Law, C. J., Wharton, R. S., et al. 2017, Natur, 541, 58
Cole, S., & Lacey, C. 1996, MNRAS, 281, 716
Connor, L., Sievers, J., & Pen, U.-L. 2016, MNRAS, 458, L19
Cordes, J. M., & Lazio, T. J. W. 2002, arXiv:astro-ph/0207156
de Graaff, A., Cai, Y.-C., Heymans, C., & Peacock, J. A. 2017, arXiv:1709.10378
Deng, W., & Zhang, B. 2014, ApJL, 783, L35
Dolag, K., Gaensler, B. M., Beck, A. M., & Beck, M. C. 2015, MNRAS, 451, 4277
Duffy, A. R., Schaye, J., Kay, S. T., & Dalla Vecchia, C. 2008, MNRAS, 390, L64
Eftekhari, T., & Berger, E. 2017, ApJ, 849, 162
Fielding, D., Quataert, E., McCourt, M., & Thompson, T. A. 2017, MNRAS, 466, 3810
Fukugita, M., & Peebles, P. J. E. 2004, ApJ, 616, 643
Gaensler, B. M., Madsen, G. J., Chatterjee, S., & Mao, S. A. 2008, PASA, 25, 184
Henriques, B. M. B., White, S. D. M., Thomas, P. A., et al. 2015, MNRAS, 451, 2663
Hogg, D. W. 1999, arXiv:astro-ph/9905116
Hopkins, A. M., & Beacom, J. F. 2006, ApJ, 651, 142
Inoue, S. 2004, MNRAS, 348, 999
Ioka, K. 2003, ApJL, 598, L79
Kokubo, M., Mitsuda, K., Sugai, H., et al. 2017, ApJ, 844, 95
Kulkarni, S. R., Ofek, E. O., & Neill, J. D. 2015, arXiv:1511.09137
Law, C. J., Bower, G. C., Burke-Spolaor, S., et al. 2018, ApJS, 236, 8
Lorimer, D. R., Bailes, M., McLaughlin, M. A., Narkevic, D. J., & Crawford, F. 2007, Sci, 318, 777
Macquart, J.-P., & Ekers, R. 2018, MNRAS, 480, 4211
McQuinn, M. 2014, ApJL, 780, L33
McQuinn, M. 2016, ARA&A, 54, 313
Michilli, D., Seymour, A., Hessels, J. W. T., et al. 2018, Natur, 553, 182
Mobasher, B., Dahlen, T., Ferguson, H. C., et al. 2015, ApJ, 808, 101
Murray, S. G., Power, C., & Robotham, A. S. G. 2013, A&C, 3, 23
Navarro, J. F., Frenk, C. S., & White, S. D. M. 1996, ApJ, 462, 563
Petroff, E., Barr, E. D., Jameson, A., et al. 2016, PASA, 33, e045
Planck Collaboration, Ade, P. A. R., Aghanim, N., et al. 2016, A&A, 594, A13
Platts, E., Weltman, A., Walters, A., et al. 2018, arXiv:1810.05836
Press, W. H., Teukolsky, S. A., Vetterling, W. T., & Flannery, B. P. 2007, Numerical Recipes 3rd Edition: The Art of Scientific Computing (3rd ed.; New York: Cambridge Univ. Press)
Prochaska, J. X., Werk, J. K., Worseck, G., et al. 2017, ApJ, 837, 169
Ravi, V., & Loeb, A. 2018, arXiv:1811.00109
Ravi, V., Shannon, R. M., Bailes, M., et al. 2016, Sci, 354, 1249
Sanidas, S., Caleb, M., Driessen, L., et al. 2018, in IAU Symp. 337, Pulsar Astrophysics the Next Fifty Years 337 (Cambridge: Cambridge Univ. Press), 406
Schaller, M., Frenk, C. S., Bower, R. G., et al. 2015, MNRAS, 451, 1247
Shannon, R. M., Macquart, J.-P., Bannister, K. W., et al. 2018, Natur, 562, 386
Sheth, R. K., Mo, H. J., & Tormen, G. 2001, MNRAS, 323, 1
Shull, J. M., & Danforth, C. W. 2018, ApJL, 852, L11
Shull, J. M., Smith, B. D., & Danforth, C. W. 2012, ApJ, 759, 23
Smail, I., Hogg, D. W., Yan, L., & Cohen, J. G. 1995, ApJL, 449, L105
Suresh, J., Rubin, K. H. R., Kannan, R., et al. 2017, MNRAS, 465, 2966
Tanimura, H., Hinshaw, G., McCarthy, I. G., et al. 2019, MNRAS, 483, 223
Tendulkar, S. P., Bassa, C. G., Cordes, J. M., et al. 2017, ApJL, 834, L7
Thornton, D., Stappers, B., Bailes, M., et al. 2013, Sci, 341, 53
Tumlinson, J., Peeples, M. S., & Werk, J. K. 2017, ARA&A, 55, 389
Walker, C. R. H., Ma, Y.-Z., & Breton, R. P. 2018, arXiv:1804.01548
Wang, L., Dutton, A. A., Stinson, G. S., et al. 2017, MNRAS, 466, 4858
Werk, J. K., Prochaska, J. X., Tumlinson, J., et al. 2014, ApJ, 792, 8
Xu, J., & Han, J. L. 2015, RAA, 15, 1629
Yang, Y.-P., Luo, R., Li, Z., & Zhang, B. 2017, ApJL, 839, L25
Zheng, Z., Ofek, E. O., Kulkarni, S. R., Neill, J. D., & Juric, M. 2014, ApJ, 797, 71